

Pedestrian Attribute Recognition via Hierarchical Cross-Modality HyperGraph Learning

Xiao Wang¹, Shujuan Wu¹, Xiaoxia Cheng^{1*}, Changwei Bi¹, Jin Tang¹, Bin Luo¹

¹School of Computer Science and Technology, Anhui University, Hefei, China

{xiaowang, tangjin, luobin}@ahu.edu.cn

{e24201114, e125221207}@stu.ahu.edu.cn, zjucxx@zju.edu.cn

Abstract

Current Pedestrian Attribute Recognition (PAR) algorithms typically focus on mapping visual features to semantic labels or attempt to enhance learning by fusing visual and attribute information. However, these methods fail to fully exploit attribute knowledge and contextual information for more accurate recognition. Although recent works have started to consider using attribute text as additional input to enhance the association between visual and semantic information, these methods are still in their infancy. To address the above challenges, this paper proposes the construction of a multi-modal knowledge graph, which is utilized to mine the relationships between local visual features and text, as well as the relationships between attributes and extensive visual context samples. Specifically, we propose an effective multi-modal knowledge graph construction method that fully considers the relationships among attributes and the relationships between attributes and vision tokens. To effectively model these relationships, this paper introduces a knowledge graph-guided cross-modal hypergraph learning framework to enhance the standard pedestrian attribute recognition framework. Comprehensive experiments on multiple PAR benchmark datasets have thoroughly demonstrated the effectiveness of our proposed knowledge graph for the PAR task, establishing a strong foundation for knowledge-guided pedestrian attribute recognition. The source code of this paper will be released on <https://github.com/Event-AHU/OpenPAR>

1. Introduction

Pedestrian Attribute Recognition (PAR) [31] targets to predict the human attributes like *long hair*, *long pants* from a given attribute set based on a given pedestrian image. It can be seen as a middle-level semantic representation and contributes to other computer vision tasks like person re-

identification [23], pedestrian detection [43], object tracking [20], and text-based person retrieval [2]. PAR has been widely deployed in practical smart video surveillance, autonomous driving, etc. However, the performance of pedestrian attribute recognition is still poor in challenging scenarios, e.g., low illumination, motion blur, and occlusion.

Current algorithms usually formulate the PAR as a multi-label classification problem and learn a mapping function from the input image to the semantic labels using the encoder-decoder framework. Specifically, DeepMAR [15] proposed by Li et al. first learning a deep neural network and predicts the pedestrian attributes in an end-to-end manner. Later, some researchers further enhanced such a framework by fusing the vision and attribute features, e.g., VTB [4], SeqPAR [13], and PromptPAR [32], as shown in Fig. 1 (a, b). Specifically, Cheng et al. first extract the vision and attribute features using the Transformer network and fuse them for high-performance PAR. After that, Wang et al. propose to enhance this framework by prompting the pre-trained multi-modal foundation model CLIP [26], Jin et al. [13] formulate the PAR as a sequence generation problem based on a Transformer network.

Despite significant progress having been made with the help of Transformer networks and foundation models, the PAR still suffers from the following issues: 1). Existing works usually model the PAR as a mapping from the given pedestrian image to the semantic labels using CNN, LSTM, or Transformers, but ignore the mining of semantic information of pedestrian attributes. Obviously, the semantic gaps will hinder the further improvement of these models. 2). Some models attempt to fuse the semantic attribute phases into the vision feature learning stage, but few of them consider the higher-order relations between the attributes and vision features. Thus, it is natural to raise the following question: “*How can we exploit the higher-order relations between the pedestrian attributes and the attribute-vision features for high-performance pedestrian attribute recognition?*”

Inspired by the success of knowledge graph [22], in this

*Corresponding Author: Xiaoxia Cheng

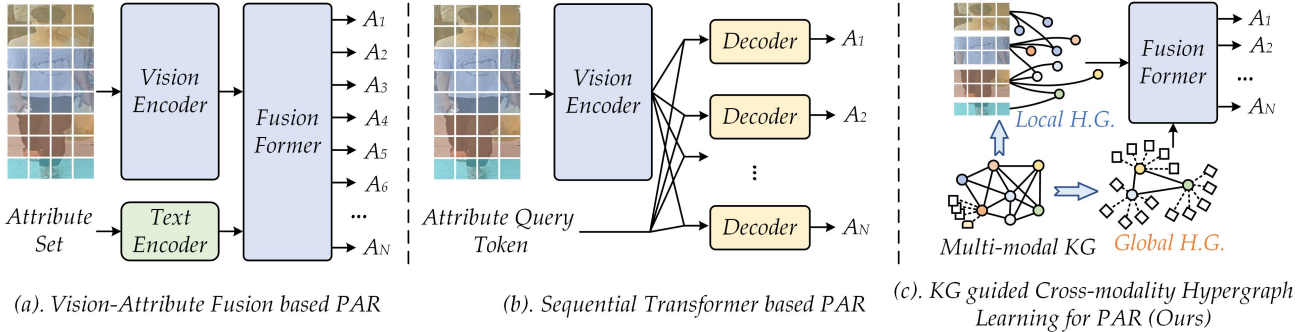


Figure 1. Comparison between existing (a). vision-text fusion based PAR, (b). sequential Transformer based PAR, and (c). our newly proposed knowledge graph guided cross-modality hypergraph learning for PAR.

paper, we attempt to bridge the semantic gap between the vision and attribute information, and achieve knowledge graph guided hierarchical cross-modal hypergraph learning for pedestrian attribute recognition. The key insight of this paper is to build a multi-modal knowledge graph that takes the human body, attributes as the entity, and trunk-attribute as the relation. It also takes the language captions of each attribute and the context vision samples as attributes of each entity to help the models better understand the attributes. As shown in Fig. 2, we enhance the standard visual-attribute mapping framework from two perspectives through the constructed multi-modal knowledge graph, namely *local patch-attribute relation mining* and *attribute-global context sampling relation mining*. We adopt the hypergraph to capture the higher-order relations in these two modules and encode them using the LA-UniGNN and AG-UniGNN networks. After that, we concatenate these processed tokens and feed them into a multi-modal Transformer for vision-semantic aggregation. Finally, we adopt a prediction head (i.e., the Feed-Forward Network, FFN) to output the predicted pedestrian attributes.

To sum up, the main contributions of this paper can be summarized as the following three aspects:

- We propose a novel multi-modal pedestrian attribute knowledge graph, termed M2PA-KG, this knowledge graph is the first large-scale multi-modal knowledge graph in the PAR domain, containing comprehensive attribute entities, human body entities, attribute descriptions, and visual context samples.
- We propose a novel Hierarchical Cross-Modal HyperGraph Learning for Knowledge Graph Augmented Pedestrian Attribute Recognition, termed KGPAR. This framework fully exploits the high-order relationships between attributes and between attributes and images, achieving knowledge-guided high-performance pedestrian attribute recognition through effective hypergraph modeling.
- Extensive experiments on multiple PAR benchmark datasets fully validated the effectiveness of our proposed

M2PA-KG for the PAR task, laying a solid foundation for knowledge-guided pedestrian attribute recognition.

2. Related Works

2.1. Pedestrian Attribute Recognition

Pedestrian Attribute Recognition (PAR)¹ aims to classify pedestrians based on attributes such as gender and clothing. Par tasks can be divided into these categories, CNN-based methods, attention- and pose-guided methods, and transformer-based methods. CNN-based methods were the earliest to dominate PAR research. These methods use convolutional neural networks such as VGG and ResNet to extract global or local visual features from pedestrian images, followed by multi-label classifiers to predict attributes. Abdulnabi et al. [1] employ CNNs for pedestrian attribute analysis and propose a multi-task learning strategy that uses multiple CNNs to learn attribute-specific features, enabling knowledge sharing across networks. Diba et al. [6] design an iterative clustering algorithm for pedestrian attribute recognition, referred to as Deep-CAMP, which progressively refines attribute-specific clusters to improve recognition performance. Later, in order to improve the spatial alignment between attributes and corresponding body regions, attention guidance and posture guidance methods were proposed. For example, HP-Net [24] combines multi-scale attention mechanisms across different semantic levels to optimize feature representation. VeSPA [27] uses the view sensitive attention mechanism to adaptively select the area Er according to the pedestrian’s perspective networks.

Transformers like ViT improved long-range dependency modeling but still encounter difficulties in capturing subtle attribute variations and addressing attribute imbalance, as demonstrated in ExpIB-Net [36] and SOFAFormer [37]. Recent works leverage multimodal learning for enhanced recognition. VTB [4] combined visual and textual features

¹<https://github.com/wangxiao5791509/Pedestrian-Attribute-Recognition-Paper-List>

through transformer architectures, and LLM-PAR [14] incorporated large language models to refine semantic reasoning. But these methods still face challenges in cross-dataset generalization.

2.2. Knowledge Graph

In recent years, Knowledge Graphs (KGs) have been widely applied across various domains due to their ability to represent complex relationships and semantic information. For instance, Google Knowledge Graph [29] enhances search accuracy through semantic understanding; IBM Watson Health [21] uses KGs to support personalized treatment recommendations in healthcare; and SR-GNN [40] in e-commerce improves recommendation systems by modeling user behavior and product attributes. Knowledge graphs have also found applications in finance, education, and other fields, demonstrating their versatile utility.

In this study, we construct a multi-modal knowledge graph to provide structured guidance for subsequent hypergraph construction. By integrating multiple modalities such as images and text, the knowledge graph effectively captures the relationships between entities, offering a solid foundation for hypergraph modeling. This multi-modal knowledge graph serves as a powerful semantic support for downstream tasks, contributing significantly to the optimization of pedestrian attribute recognition.

3. Methodology

3.1. Overview

The overall framework of our architecture is illustrated in Fig. 2. Our method first obtains input embeddings through CLIP §3.2. and constructs a multi-modal knowledge graph to capture semantic and structural relationships among visual attributes §3.3. To further model both the internal topological structure of individual images and the semantic correlations across images, we design a hierarchical cross-modal hypergraph learning mechanism §3.4. Finally, the learned representations are integrated for attribute prediction §3.5.

3.2. Input Embedding

In this work, we adopt the image encoder $f(\cdot)$ and text encoder $g(\cdot)$ from CLIP as feature extractors for vision and language, respectively. Formally, given an image x^v , we first apply a patch embedding layer $\text{PatchEmbed}(\cdot)$ to split the input image x^v and project it into fixed-size patch embeddings $v_p = [v_p^1, v_p^2, \dots, v_p^N] \in \mathbb{R}^{N \times d}$, where N is the number of image patches, and d is the feature dimension.

To model local region semantics, the input image is horizontally divided into R regions (e.g., head, upper, lower, foot), and a corresponding learnable d -dimensional token CLS_{l_i} is assigned to each region. In addi-

tion, following existing methods, we introduce a learnable d -dimensional global classification token CLS_g . Therefore, we get the complete input sequence $v_{all} = [\text{CLS}_g; \text{CLS}_{l_1}, \text{CLS}_{l_2}, \dots, \text{CLS}_{l_R}; v_p]$. Feeding this sequence into the image encoder $f(\cdot)$ to get the final input embeddings:

$$[c_g; c_{l_1}, \dots, c_{l_R}; h_p] = f(v_{all}), \quad (1)$$

where c_g , c_{l_i} , and h_p are the global embedding, local embeddings, and the patch-level embeddings, respectively. These embeddings are in a shared embedding space enabling alignment with text modalities and facilitating downstream tasks.

3.3. Multi-modal Knowledge Graph Construction

To capture the semantic and structural relationships among attributes, we construct a multi-modal knowledge graph for each dataset, as shown in Fig. 3. This knowledge graph serves as the foundation for subsequent learning tasks. Formally, the knowledge graph is defined as:

$$G = (V, E, S, I) \quad (2)$$

where V , E , S , and I represent the set of nodes, edges, textual features, and visual features, respectively. Each pedestrian attribute is modeled as a node and systematically organized into five semantic modules: head, body, upper body, lower body, and foot. Every node is associated with both textual and visual representations, while edges are established according to the co-occurrence patterns of attributes observed in the dataset.

Specifically, we construct an attribute co-occurrence adjacency matrix $A \in \mathbb{R}^{M \times M}$ by aggregating attribute labels across all images:

$$A_{ij} = \sum_{k=1}^N L_{ki} \cdot L_{kj}, \quad (3)$$

where $L \in \{0, 1\}^{N \times M}$ denotes the label matrix, and A_{ii} indicates the frequency of attribute i . This adjacency matrix serves to establish edges between nodes in the knowledge graph. To facilitate the propagation of multimodal features, we perform row-wise normalization of the adjacency matrix:

$$\tilde{A}_{ij} = \frac{A_{ij}}{A_{ii}}, \quad A_{ii} > 0. \quad (4)$$

Each element \tilde{A}_{ij} of the normalized matrix is employed as the edge weight between nodes i and j , reflecting the strength of their association.

This knowledge graph not only preserves the semantic and visual correlations among attributes but also provides explicit guidance for the construction of local and global hypergraphs, thereby promoting efficient interaction and propagation of multimodal features.

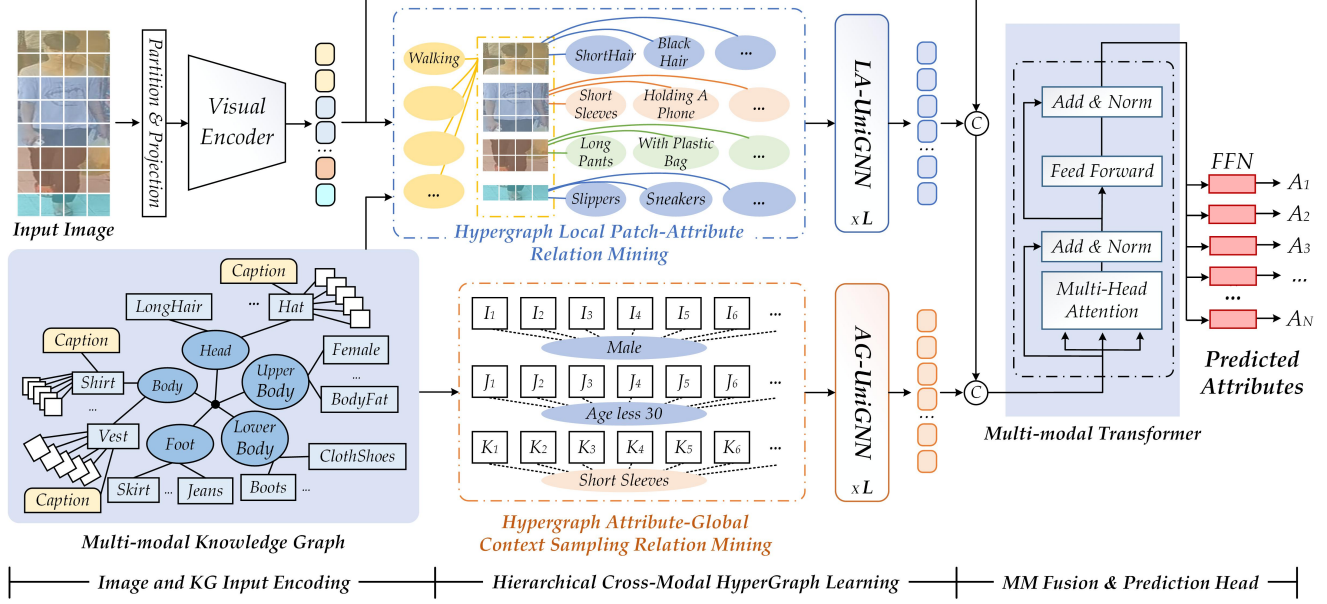


Figure 2. An overview of our proposed knowledge graph augmented PAR by learning the hierarchical cross-modal hypergraph.

3.4. Hierarchical Cross-modal HyperGraph Learning

To capture the internal topological structure of individual images and the semantic relationships across images, we design a hierarchical cross-modal hypergraph learning mechanism. Within this mechanism, we construct both local and global hypergraphs to effectively model intra-image feature interactions and inter-image correlations.

• **Local HyperGraph** As demonstrated in Section 3.3, each pedestrian image is first divided into several predefined regions $R = \{\text{body}, \text{head}, \text{upper}, \text{lower}, \text{foot}\}$. To establish semantic correspondences between text $T_r = \{t_1, \dots, t_{M_r}\}$ and visual $h_{p_r} = \{h_{p_1}, \dots, h_{p_{N_r}}\}$ within each region $r \in R$, we compute the similarity matrix:

$$S_r = \mathbf{h}_{p_r} \cdot T_r^\top \in \mathbb{R}^{N_r \times M_r}. \quad (5)$$

For each textual token $t_j \in T_r$, only the visual patch tokens $\mathbf{h}_{p_i} \in \mathbf{h}_p$ whose similarity exceeds a threshold τ are retained. These selected patch tokens are then combined with the corresponding textual token to form a hyperedge, thereby constructing a region-level hypergraph.

Finally, all regional hypergraph nodes and hyperedges are merged to form the complete local hypergraph. This hypergraph is then input into the UniGNN[9] for encoding, producing region features $\mathbf{H}_{\text{local}}$ that capture the fused text-visual semantic relationships.

• **Global HyperGraph** To jointly model the semantic alignment between images and attribute texts, we construct a Global HyperGraph. The attribute texts are mapped into a shared feature space using the CLIP text encoder, yield-

ing the text embedding matrix $F_{\text{text}} = [f_1^{\text{text}}, f_2^{\text{text}}, \dots, f_M^{\text{text}}]$, where d denotes the embedding dimension. For the image collection, global class tokens extracted by the CLIP visual encoder serve as semantic representations, forming the image embedding matrix $F_{\text{img}} = [f_1^{\text{img}}, f_2^{\text{img}}, \dots, f_N^{\text{img}}]$. By concatenating image and text features, we obtain the node feature matrix of the global hypergraph

$$F = \begin{bmatrix} F_{\text{img}} \\ F_{\text{text}} \end{bmatrix} \in \mathbb{R}^{(N+M) \times d}. \quad (6)$$

To capture the image-text correspondence, an image-to-attribute association matrix $Y_{\text{img}} \in \mathbb{R}^{N \times M}$ is constructed, where

$$Y_{\text{img}}[i, j] = \begin{cases} 1, & \text{if image } I_i \text{ is associated with attribute } t_j, \\ 0, & \text{otherwise.} \end{cases} \quad (7)$$

To maintain the independence of text nodes, an identity matrix $Y_{\text{text}} = I_M \in \mathbb{R}^{M \times M}$ is introduced. Consequently, the association matrix A of the global hypergraph is constructed as follows:

$$A = \begin{bmatrix} Y_{\text{img}} \\ Y_{\text{text}} \end{bmatrix} \in \mathbb{R}^{(N+M) \times M}. \quad (8)$$

The constructed global hypergraph is then input into UniGNN[9] for encoding, generating image-text aligned representations $\mathbf{H}_{\text{global}}$ that capture global semantic relationships.

3.5. Attributes Prediction

Before performing prediction, we apply a multi-modal fusion strategy to integrate the visual features derived from

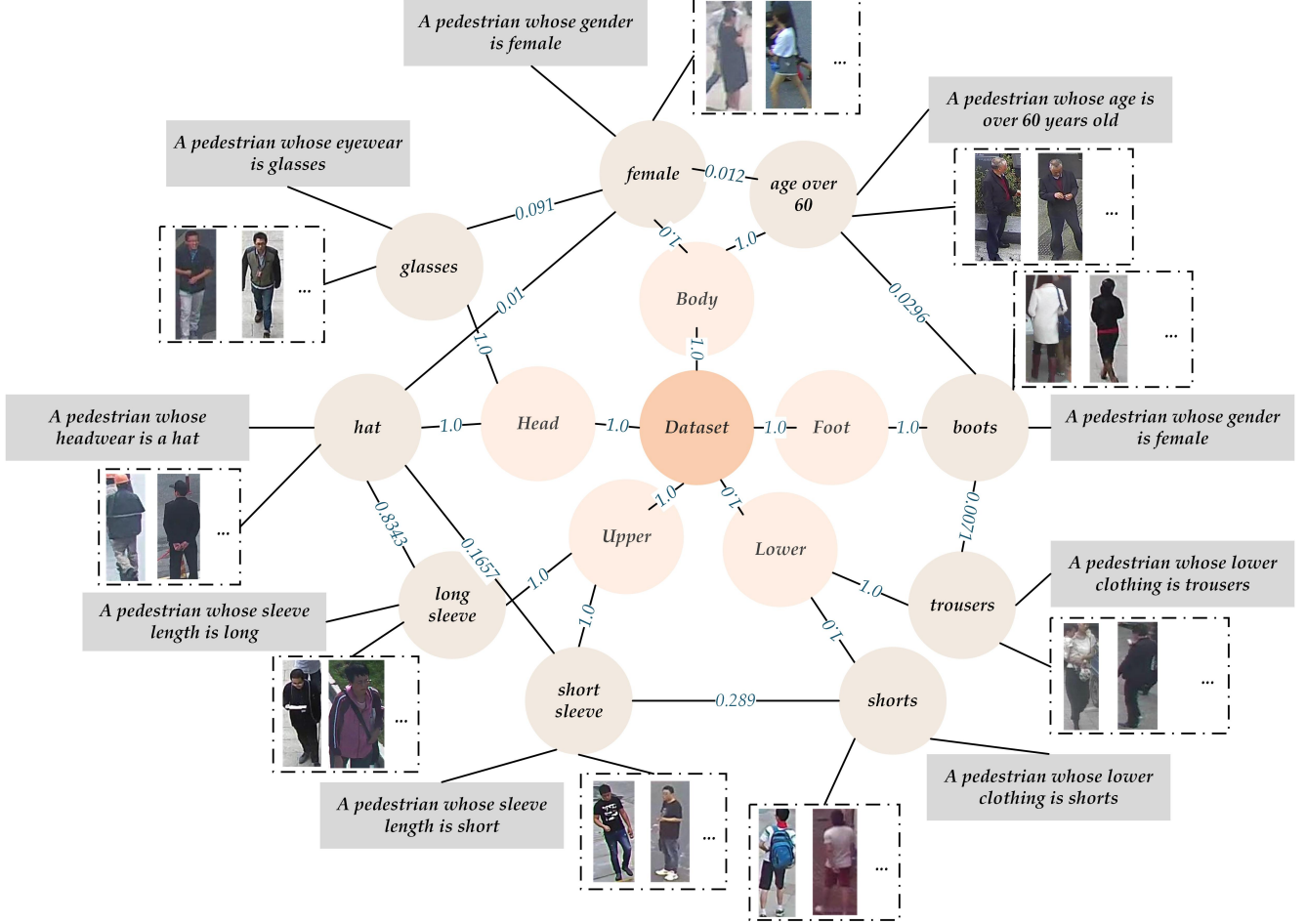


Figure 3. An overview of the built knowledge graph for pedestrian attribute recognition.

both the global and local hypergraphs.

- **Multi-modal Fusion** Inspired by VTB [4], we concatenate the visual features with the constructed global hypergraph and local hypergraph, and feed them into a multi-modal Transformer for joint modeling and deep interaction across different modalities. Specifically, the concatenated input sequence is:

$$Z = [\mathbf{H}_{\text{local}}; \mathbf{H}_{\text{global}}; f(v_{\text{all}})]. \quad (9)$$

The multi-head self-attention mechanism enables the Transformer to capture high-order dependencies across modalities while integrating structural information at different granularities. After this fusion, the model obtains more discriminative multi-modal representations, which ultimately enhance attribute prediction.

- **Prediction** Based on the representations obtained from the Multi-modal Fusion, we employ a feed-forward network (FFN) as the classifier to regress attribute scores:

$$R = \text{FFN}(Z) = \sigma(wZ + b) \quad (10)$$

where w and b denote the weight and bias of the FFN, and $\sigma(\cdot)$ is the Sigmoid activation function for producing the final attribute probabilities.

- **Loss Computation** In this study, we employ a loss function composed of two components to optimize the training process. The first is the Global-Local Similarity Loss (L_{GL}), which models the similarity between the global CLS token, local region CLS tokens, and attribute representations, and aligns them with the ground truth. This loss effectively evaluates the semantic consistency of visual features at both global and local levels. It is formulated as a binary cross-entropy function:

$$L_{GL} = -\frac{1}{M} \sum_{i=1}^M \sum_{j=1}^N (y_{ij} \log(p_{ij}^{GL}) + (1 - y_{ij}) \log(1 - p_{ij}^{GL})) \quad (11)$$

where p_{ij}^{GL} denotes the similarity prediction of the i -th sample for the j -th attribute, and y_{ij} represents the corresponding ground truth label. This loss ensures that attribute embeddings achieve semantic alignment at both global and local levels.

cal levels. The second is the Weighted Cross-Entropy Loss (L_{CLS}), which addresses the class imbalance commonly encountered in pedestrian attribute recognition. The weight for each attribute class is determined according to its frequency in the training set, defined as $w_j = e^{-r_j}$, where r_j denotes the occurrence ratio of the j -th attribute. The loss is defined as:

$$L_{CLS} = -\frac{1}{M} \sum_{i=1}^M \sum_{j=1}^N w_j (y_{ij} \log(p_{ij}) + (1 - y_{ij}) \log(1 - p_{ij})) \quad (12)$$

where p_{ij} indicates the predicted probability of the j -th attribute for the i -th image. By incorporating this weighting scheme, the loss function reduces the dominance of majority classes in the optimization process, thereby enhancing the recognition capability for minority attributes. The final overall optimization objective is formulated as:

$$L = L_{CLS} + \alpha L_{GL} \quad (13)$$

where α is a trade-off parameter that balances classification performance and global-local alignment.

4. Experiments

4.1. Datasets and Evaluation Metric

To demonstrate the effectiveness of our proposed method, we conduct experiments on five PAR benchmark datasets, including standard PETA [5], PA100K [24], RAPv1 [17], RAPv2 [18], MSP60K [14]. We adopt five widely used evaluation metrics to rigorously assess model performance: mean Accuracy (mA), Accuracy (Acc), Precision (Prec), Recall, and F1-score (F1).

4.2. Implementation Details

During the training phase, we employ the ViT-L/14 version of CLIP as the visual encoder, with input images resized to 224×224 . The model is trained with a batch size of 16 for a total of 100 epochs. This training configuration is consistently applied across the RAPv1, RAPv2, PETA, and PA100K datasets. The initial learning rate is set to $7e-4$ and decays progressively at a rate of $1e-4$, while an additional 0.01 learning rate decay is applied to stabilize the training process. Parameter updates are performed using the AdamW optimizer. Further implementation details are available in our source code.

4.3. Comparison on Public Benchmarks

- **Results on PETA [5] dataset.** Our method achieves 88.50, 83.27, 89.74, 89.56, and 89.43 in mA, Accuracy, Precision, Recall, and F1, respectively. Although it does not surpass methods such as DRFormer or OAGCN on individual metrics, the overall performance remains consistently

high, demonstrating a well-balanced capability across metrics.

- **Results on PA100K [24] dataset.** Our approach reaches 87.95, 84.01, 89.55, 91.65, and 90.28 in mA, Accuracy, Precision, Recall, and F1, respectively. Compared with FRDL, it achieves improvements of 1.65 and 2.36 on mA and F1, respectively; it also outperforms PARformer in terms of Accuracy and F1.

- **Results on RAPv1 [17] dataset.** Our method obtains 85.46, 71.81, 80.54, 85.16, and 82.46 in mA, Accuracy, Precision, Recall, and F1, respectively. Compared with OAGCN, it achieves comparable or even superior results without relying on additional viewpoint information.

- **Results on RAPv2 [18] dataset.** The results are 83.02, 70.03, 78.33, 85.17, and 81.27 in mA, Accuracy, Precision, Recall, and F1, respectively. Although Accuracy is slightly lower than some other methods, the performance in mA and F1 remains competitive.

- **Results on MSP60K [14] datasets.** We evaluated our method on the MSP60K dataset, and the experimental results are shown in Table 3. In the random split, our method achieved mA 79.03, Acc 76.94, Precision 84.14, Recall 88.14, and F1 85.69. In the cross-domain split, our method achieved mA 63.82, Acc 53.67, Precision 65.86, Recall 72.35, and F1 68.41, demonstrating stable performance. These results demonstrate that our method exhibits excellent performance on the MSP60K dataset, with well-balanced and strong capabilities across multiple key metrics, validating its effectiveness and stability in cross-domain pedestrian attribute recognition tasks.

4.4. Ablation Study

- **Component Analysis.** In this experiment, we employ CLIP as the pre-trained model to extract textual and visual features. To evaluate the effectiveness of our approach, we compare it with the baseline VTB model, in which the textual module is replaced by local and global hypergraphs. All models are trained on the RAPv1 and PETA datasets to ensure fair and consistent evaluation. Table 4 summarizes the performance of each model in terms of accuracy (Acc), mean accuracy (mA), precision (Prec), recall (Rec), and F1-score.

- **Effect of Different HyperGraph Encoders.** Table 5 presents the results of using different hypergraph encoders for pedestrian attribute recognition on the RAPv1 dataset. We compared several hypergraph encoders based on the UniGNN [9] framework, including UniGIN, UniGCN, UniGAT, and the improved UniGCN2. Each encoder employs a different graph neural network approach—graph isomorphism network (UniGIN), graph convolutional network (UniGCN), graph attention mechanism (UniGAT), and the enhanced UniGCN2—demonstrating their effectiveness in pedestrian attribute recognition tasks.

Table 1. Comparison with state-of-the-art methods on PETA and PA100K datasets. The best and second best results are highlighted in **bold** and underlined, respectively. Missing values are marked with “-”.

Methods	Publish	PETA					PA100K				
		mA	Acc	Prec	Rec	F1	mA	Acc	Prec	Rec	F1
SSCNet [10]	ICCV21	86.52	78.95	86.02	87.12	86.99	81.87	78.89	85.98	89.10	86.87
CAS [41]	IJCV21	86.40	79.93	87.03	87.33	87.18	82.86	79.64	86.81	87.79	85.18
IAA [35]	PR22	85.27	78.04	86.08	85.80	85.64	81.94	80.31	88.36	88.01	87.80
DRFormer [30]	NC22	89.96	81.30	85.68	91.08	88.30	82.47	80.27	87.60	88.49	88.04
VAC [8]	IJCV22	-	-	-	-	-	82.19	80.66	88.72	88.10	88.41
DAFL [12]	AAAI22	87.07	78.88	85.78	87.03	86.40	83.54	80.13	87.01	89.19	88.09
VTB [4]	TCSVT22	85.31	79.60	86.76	87.17	86.71	83.72	80.89	87.88	89.30	88.21
PARformer [7]	TCSVT23	89.32	82.86	88.06	91.98	89.06	84.46	81.13	88.09	91.67	88.52
OAGCN [25]	TMM23	89.91	82.95	88.26	89.10	88.68	83.74	80.38	84.55	90.42	87.39
SSPNet [28]	PR24	88.73	82.80	88.48	90.55	89.50	83.58	80.63	87.79	89.32	88.55
SOFA [37]	AAAI24	87.10	81.10	87.80	88.40	87.80	83.40	81.10	88.40	89.00	88.30
FRDL [46]	ICML24	88.59	-	-	-	89.03	89.44	-	-	-	88.05
PromptPAR [32]	TCSVT24	88.76	82.84	89.04	89.74	89.18	87.47	83.78	89.27	<u>91.70</u>	90.15
SequencePAR [13]	PR25	-	84.92	90.44	90.73	90.46	-	83.94	90.38	90.23	90.10
EVSITP [38]	CVPR25	<u>89.65</u>	<u>83.93</u>	89.67	90.73	<u>90.20</u>	<u>88.66</u>	84.54	<u>89.90</u>	92.09	90.98
HDFL [39]	NN25	87.55	79.66	87.08	87.16	86.85	84.92	80.23	87.45	88.74	87.72
FOCUS [3]	ICME25	88.04	81.96	88.56	89.07	88.54	83.90	81.23	89.29	88.97	88.41
KGPAR (Ours)	-	88.50	83.27	<u>89.74</u>	89.56	89.43	87.95	<u>84.01</u>	89.55	91.65	<u>90.28</u>

Table 2. Comparison with state-of-the-art methods on RAPv1 and RAPv2 datasets. The best and second best results are highlighted in **bold** and underlined, respectively. Missing values are marked with “-”.

Methods	Publish	RAPv2					RAPv1				
		mA	Acc	Prec	Rec	F1	mA	Acc	Prec	Rec	F1
SSCNet [10]	ICCV21	-	-	-	-	-	82.77	68.37	75.05	<u>87.49</u>	80.43
CAS [41]	IJCV21	-	-	-	-	-	84.18	68.59	77.56	83.81	80.56
IAA [35]	PR22	79.99	68.03	78.75	81.37	79.69	81.72	68.47	79.56	82.06	80.37
DRFormer [30]	NC22	-	-	-	-	-	81.81	70.60	80.12	82.77	81.42
VAC [8]	IJCV22	79.23	64.51	<u>75.77</u>	79.43	77.10	81.30	70.12	<u>81.56</u>	81.51	81.54
DAFL [12]	AAAI22	81.04	66.70	76.39	82.07	79.13	83.72	68.18	77.41	83.39	80.29
VTB [4]	TCSVT22	81.34	67.48	76.41	83.32	79.35	82.67	69.44	78.28	84.39	80.84
PARformer [7]	TCSVT23	-	-	-	-	-	84.43	69.94	79.63	88.19	81.35
OAGCN [25]	TMM23	-	-	-	-	-	87.83	69.32	78.32	87.29	<u>82.56</u>
SSPNet [28]	PR24	-	-	-	-	-	83.24	70.21	80.14	82.90	81.50
SOFA [37]	AAAI24	81.9	68.6	78.0	83.1	80.2	83.40	70.00	80.00	83.00	81.20
FRDL [46]	ICML24	-	-	-	-	-	<u>87.72</u>	-	-	-	79.16
PromptPAR [32]	TCSVT24	<u>83.14</u>	69.62	77.42	85.73	81.00	85.45	71.61	79.64	86.05	82.38
SequencePAR [13]	PR25	-	70.14	81.37	81.22	81.10	-	71.47	82.40	82.09	82.05
EVSITP [38]	CVPR25	83.83	69.32	77.64	85.13	81.21	86.10	<u>71.64</u>	79.24	86.65	82.78
HDFL [39]	NN25	81.81	68.22	78.30	82.18	79.85	83.68	70.49	80.25	83.55	81.51
FOCUS [3]	ICME25	-	-	-	-	-	83.45	70.14	80.10	85.18	80.91
KGPAR (Ours)	-	83.02	<u>70.03</u>	<u>78.33</u>	<u>85.17</u>	81.27	85.05	71.75	79.95	85.98	82.50

• **Effect of Different Backbone Architectures.** Table 6 presents a comparative analysis of different backbone networks on the PA100k dataset. Replacing the ViT-B/16 backbone with the larger ViT-L/14 consistently improves

all evaluation metrics, including mean accuracy (mA), overall accuracy (Acc), precision (Prec), recall, and F1 score. Specifically, ViT-L/14 achieves 87.95% mA and 90.28% F1, outperforming ViT-B/16 by 3.6% and 1.67%, respec-

Table 3. Comparison with state-of-the-art methods on MSP60K datasets. The best and second best results are highlighted in **bold** and underlined, respectively. Missing values are marked with “-”.

Methods	Publish	Random Split					Cross-domain Split				
		mA	Acc	Prec	Recall	F1	mA	Acc	Prec	Recall	F1
DeepMAR [16]	ACPR15	70.46	72.83	84.71	81.46	83.06	54.84	44.97	63.38	58.81	61.01
RethinkingPAR [11]	arXiv20	74.01	74.20	84.17	83.94	84.06	55.98	46.52	62.85	62.09	62.47
SSCNet [10]	ICCV21	69.71	69.31	79.22	82.47	80.82	52.84	40.88	56.26	58.64	57.43
VTB [4]	TCSVT22	76.09	75.36	83.56	86.46	84.56	58.59	49.81	65.11	66.11	65.00
Label2Label [19]	ECCV22	73.61	72.66	81.79	84.32	82.56	56.38	45.81	59.67	64.20	61.19
DFDT [44]	EAAI22	74.19	76.35	85.03	86.35	85.69	57.85	49.97	65.34	66.18	65.76
Zhou et al. [45]	IJCAI23	73.07	68.76	78.38	82.10	80.20	54.26	41.91	56.23	60.11	58.11
PARformer [7]	TCSVT23	76.14	76.67	84.77	86.93	85.44	57.96	50.63	62.28	71.04	65.82
VTB-PLIP [47]	arXiv23	73.90	73.16	82.01	84.82	82.93	56.30	46.77	61.20	64.47	62.18
Rethink-PLIP [47]	arXiv23	69.44	68.90	79.82	81.15	80.48	57.18	46.98	63.57	62.16	62.86
PromptPAR [32]	TCSVT24	78.81	76.53	<u>84.40</u>	87.15	85.35	63.24	53.62	66.15	71.84	68.32
SSPNet [28]	PR24	74.03	74.10	84.01	84.02	84.02	56.15	46.75	62.44	63.07	62.75
HAP [42]	NIPS24	76.92	76.12	84.78	86.14	85.45	58.70	50.59	65.60	66.91	66.25
MambaPAR [34]	arXiv24	73.85	73.64	83.19	84.29	83.28	56.75	47.34	61.92	64.98	62.80
MaHDFT [33]	arXiv24	74.08	74.40	82.82	86.41	83.93	58.67	50.65	62.39	71.13	65.85
SequencePAR [13]	PR25	71.88	71.99	83.24	82.29	82.29	57.88	50.27	65.81	65.79	65.37
LLM-PAR [14]	AAAI25	80.13	78.71	84.39	90.52	86.94	66.29	58.11	65.68	81.21	72.05
KGPAR (Ours)	-	79.03	<u>76.94</u>	84.14	<u>88.14</u>	<u>85.69</u>	63.82	<u>53.67</u>	<u>65.86</u>	72.35	68.41

Table 4. Ablation Study on RAPv1, and PETA datasets

#	Baseline	Local-HG	Global-HG	RAPv1					PETA				
				mA	Acc	Prec	Recall	F1	mA	Acc	Prec	Recall	F1
1	✓			83.58	70.02	78.63	84.87	81.24	87.05	81.18	88.29	88.05	87.93
2	✓		✓	85.28	71.19	79.51	85.66	82.11	88.54	82.02	88.65	89.04	88.60
3	✓		✓	84.78	71.36	79.31	86.16	82.24	87.98	82.13	88.58	89.43	88.75
4	✓	✓	✓	85.05	71.75	79.95	85.98	82.50	88.50	83.27	89.74	89.56	89.43

Table 5. Comparison of different HyperGraph Encoders architectures on the RAPV1 dataset for pedestrian attribute recognition.

KG Encoders	mA	Acc	Prec	Recall	F1
UniGIN	85.30	71.64	79.53	86.29	82.41
UniGCN	85.36	71.46	79.43	86.14	82.30
UniGAT	85.48	71.58	79.72	85.91	82.36
UniGCN2	85.05	71.75	79.95	85.98	82.50

tively. This performance gain can be attributed to the greater representational capacity of ViT-L/14, which allows the model to better capture fine-grained pedestrian attributes. In contrast, the smaller ViT-B/16 backbone may underrepresent complex attribute interactions, leading to slightly lower precision and recall. Overall, these results highlight the importance of backbone selection in pedestrian attribute recognition, as larger models can more effectively encode

discriminative features and enhance recognition robustness across diverse scenarios.

Table 6. Comparison of different backbone architectures on the PA100K dataset for pedestrian attribute recognition.

Backbone	mA	Acc	Prec	Recall	F1
ViT-B/16	84.35	81.45	88.16	89.79	88.61
ViT-L/14	87.95	84.01	89.55	91.65	90.28

- Effect of Different Number of Vision Context Samples.** Table 7 presents the effect of varying the number of images applied to each node’s visual attributes on pedestrian attribute recognition performance using the RAPv1 dataset. During knowledge graph construction, a fixed number of images are assigned to each node’s visual attributes. This experiment compares the impact of different image quantities on the performance of the method.

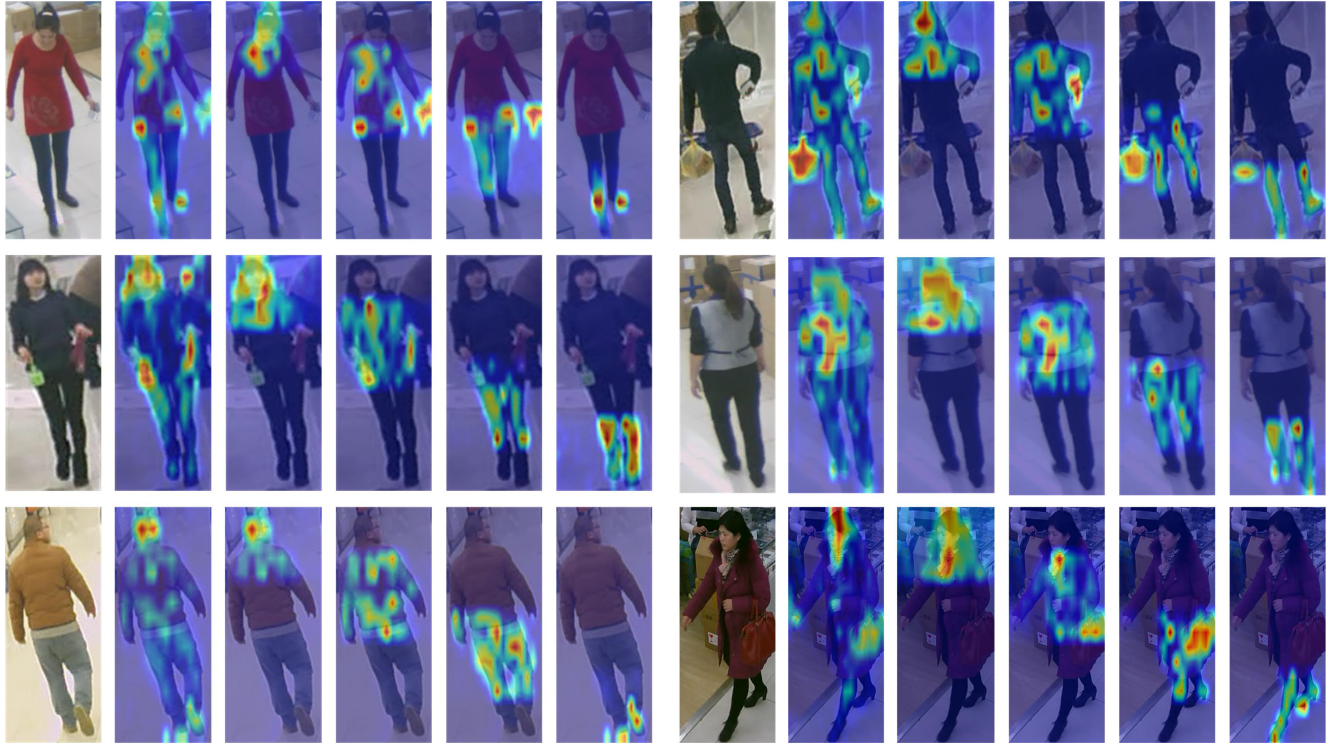


Figure 4. Visualization of heat maps given the corresponding pedestrian attribute.



Figure 5. Visualization of our predicted attribute results.

• **Effect of Different Regional Partitioning Methods.** Table 8 presents a comparative analysis of regional versus non-regional partitioning strategies on the RAPv2 dataset. The regional division method achieves slightly higher mean

accuracy (mA) and F1 score compared to the non-regional approach, with 83.02% mA and 81.27% F1. This indicates that explicitly dividing the image into semantic regions can help the model capture localized attribute fea-

Table 7. Comparison of the effect of the number of images applied to each node in the knowledge graph on pedestrian attribute recognition performance on the RAPv1 dataset.

number	mA	Acc	Prec	Recall	F1
2	85.22	71.60	79.86	85.79	82.39
4	85.09	71.48	79.28	86.31	82.30
6	84.93	71.26	79.47	85.76	82.14
8	84.81	71.09	79.01	86.08	82.04
10	85.05	71.75	79.95	85.98	82.50

tures more effectively. However, the non-regional method exhibits marginally higher recall (85.37% vs. 85.17%), suggesting that global features may sometimes provide complementary information for certain attributes. Overall, incorporating regional partitioning improves the model’s ability to focus on fine-grained attribute details while maintaining competitive overall performance, demonstrating its usefulness in pedestrian attribute recognition tasks.

Table 8. Comparison of regional and non-regional partitioning methods on the RAPv2 dataset for pedestrian attribute recognition.

Regional Method	mA	Acc	Prec	Recall	F1
Regional division	83.02	70.03	78.33	85.17	81.27
non Regional division	83.37	69.50	77.53	85.37	80.91

4.5. Visualization

• **Heatmap Visualization.** To provide a more comprehensive illustration of the model’s visual attention mechanism when predicting pedestrian attributes on the RAPV1 dataset, we adopt a heatmap-based visualization to highlight the critical response regions. As illustrated in Fig. 4, the model effectively attends to semantically relevant regions that are highly correlated with different attributes during inference, thereby demonstrating strong interpretability and a robust discriminative capability in attribute-specific feature localization.

• **Attributes Predicted.** As illustrated in Fig. 5, this work provides multiple examples of attribute recognition results on the RAPV1 dataset. Both quantitative and qualitative analyses indicate that the model achieves high stability and accuracy in identifying several key attribute categories, including gender, age, and clothing style. Even in complex scenarios, the model demonstrates consistent robustness in recognizing common attributes.

4.6. Limitation Analysis

The model achieves competitive results but has some limitations. It relies on predefined body region partitions, which

limits its ability to capture fine-grained attributes, particularly for accessories or complex textures. The fixed thresholds for constructing hypergraphs may not fully capture rare attributes, leading to suboptimal performance in such cases. Additionally, datasets like PETA and PA100K suffer from annotation inconsistencies and imbalances, which affect generalization. Lastly, the computational overhead from cross-modal hypergraphs may hinder large-scale real-time deployment. Future work will focus on adaptive partitioning, improved hypergraph construction, and lightweight variants for better efficiency.

5. Conclusion

We propose KGPAR, a hierarchical cross-modal hypergraph framework for pedestrian attribute recognition. By combining local and global hypergraph learning, it effectively captures intra-image feature interactions and inter-sample semantic relationships between visual and textual modalities. Extensive experiments on PETA, PA100K, RAPv1, RAPv2, and MSP60K demonstrate competitive performance across all metrics, showcasing improved robustness and balanced prediction. Future work will explore dynamic hypergraph construction and more efficient learning to enhance cross-dataset generalization and real-time applicability.

References

- [1] Abrar H Abdulnabi, Gang Wang, Jiwen Lu, and Kui Jia. Multi-task cnn model for attribute prediction. *IEEE Transactions on Multimedia*, 17(11):1949–1959, 2015.
- [2] Surbhi Aggarwal, Venkatesh Babu Radhakrishnan, and Anirban Chakraborty. Text-based person search via attribute-aided matching. In *Proceedings of the IEEE/CVF winter conference on applications of computer vision*, pages 2617–2625, 2020.
- [3] Hongyan An, Kuan Zhu, Xin He, Haiyun Guo, Chaoyang Zhao, Ming Tang, and Jinqiao Wang. Focus: Fine-grained optimization with semantic guided understanding for pedestrian attributes recognition. *arXiv preprint arXiv:2506.22836*, 2025.
- [4] Xinhua Cheng, Mengxi Jia, Qian Wang, and Jian Zhang. A simple visual-textual baseline for pedestrian attribute recognition. *IEEE Transactions on Circuits and Systems for Video Technology*, 32(10):6994–7004, 2022.
- [5] Yubin Deng, Ping Luo, Chen Change Loy, and Xiaoou Tang. Pedestrian attribute recognition at far distance. In *Proceedings of the 22nd ACM international conference on Multimedia*, pages 789–792, 2014.
- [6] Ali Diba, Ali Mohammad Pazandeh, Hamed Pirsiavash, and Luc Van Gool. Deepcamp: Deep convolutional action & attribute mid-level patterns. In *Proceedings of the IEEE Conference on Computer Vision and Pattern Recognition*, pages 3557–3565, 2016.

[7] Xinwen Fan, Yukang Zhang, Yang Lu, and Hanzi Wang. Parformer: Transformer-based multi-task network for pedestrian attribute recognition. *IEEE Transactions on Circuits and Systems for Video Technology*, 34(1):411–423, 2023.

[8] Hao Guo, Xiaochuan Fan, and Song Wang. Visual attention consistency for human attribute recognition. *International Journal of Computer Vision*, 130(4):1088–1106, 2022.

[9] Jing Huang and Jie Yang. Unignn: a unified framework for graph and hypergraph neural networks. *arXiv preprint arXiv:2105.00956*, 2021.

[10] Jian Jia, Xiaotang Chen, and Kaiqi Huang. Spatial and semantic consistency regularizations for pedestrian attribute recognition. In *Proceedings of the IEEE/CVF international conference on computer vision*, pages 962–971, 2021.

[11] Jian Jia, Houjing Huang, Xiaotang Chen, and Kaiqi Huang. Rethinking of pedestrian attribute recognition: A reliable evaluation under zero-shot pedestrian identity setting. *arXiv preprint arXiv:2107.03576*, 2021.

[12] Jian Jia, Naiyu Gao, Fei He, Xiaotang Chen, and Kaiqi Huang. Learning disentangled attribute representations for robust pedestrian attribute recognition. In *Proceedings of the AAAI Conference on Artificial Intelligence*, pages 1069–1077, 2022.

[13] Jiandong Jin, Xiao Wang, Yin Lin, Chenglong Li, Lili Huang, Aihua Zheng, and Jin Tang. Sequencepar: Understanding pedestrian attributes via a sequence generation paradigm. *Pattern Recognition*, page 112356, 2025.

[14] Jiandong Jin, Xiao Wang, Qian Zhu, Haiyang Wang, and Chenglong Li. Pedestrian attribute recognition: A new benchmark dataset and a large language model augmented framework. In *Proceedings of the AAAI Conference on Artificial Intelligence*, pages 4138–4146, 2025.

[15] Dangwei Li, Xiaotang Chen, and Kaiqi Huang. Multi-attribute learning for pedestrian attribute recognition in surveillance scenarios. In *2015 3rd IAPR Asian Conference on Pattern Recognition (ACPR)*, pages 111–115. IEEE, 2015.

[16] Dangwei Li, Xiaotang Chen, and Kaiqi Huang. Multi-attribute learning for pedestrian attribute recognition in surveillance scenarios. In *2015 3rd IAPR Asian Conference on Pattern Recognition (ACPR)*, pages 111–115. IEEE, 2015.

[17] Dangwei Li, Zhang Zhang, Xiaotang Chen, Haibin Ling, and Kaiqi Huang. A richly annotated dataset for pedestrian attribute recognition. *arXiv preprint arXiv:1603.07054*, 2016.

[18] Dangwei Li, Zhang Zhang, Xiaotang Chen, and Kaiqi Huang. A richly annotated pedestrian dataset for person retrieval in real surveillance scenarios. *IEEE transactions on image processing*, 28(4):1575–1590, 2018.

[19] Wanhua Li, Zhixuan Cao, Jianjiang Feng, Jie Zhou, and Jiwen Lu. Label2label: A language modeling framework for multi-attribute learning. In *European conference on computer vision*, pages 562–579. Springer, 2022.

[20] Yunhao Li, Zhen Xiao, Lin Yang, Dan Meng, Xin Zhou, Heng Fan, and Libo Zhang. Attmot: improving multiple-object tracking by introducing auxiliary pedestrian attributes. *IEEE transactions on neural networks and learning systems*, 36(3):5454–5468, 2024.

[21] Huiying Liang, Brian Y Tsui, Hao Ni, Carolina CS Valentim, Sally L Baxter, Guangjian Liu, Wenjia Cai, Daniel S Kermany, Xin Sun, Jiancong Chen, et al. Evaluation and accurate diagnoses of pediatric diseases using artificial intelligence. *Nature medicine*, 25(3):433–438, 2019.

[22] Wanying Liang, Pasquale De Meo, Yong Tang, and Jia Zhu. A survey of multi-modal knowledge graphs: Technologies and trends. *ACM Computing Surveys*, 56(11):1–41, 2024.

[23] Yutian Lin, Liang Zheng, Zhenzhong Zheng, Yu Wu, Zhi-lan Hu, Chenggang Yan, and Yi Yang. Improving person re-identification by attribute and identity learning. *Pattern recognition*, 95:151–161, 2019.

[24] Xihui Liu, Haiyu Zhao, Maoqing Tian, Lu Sheng, Jing Shao, Shuai Yi, Junjie Yan, and Xiaogang Wang. Hydraplus-net: Attentive deep features for pedestrian analysis. In *Proceedings of the IEEE international conference on computer vision*, pages 350–359, 2017.

[25] Wei-Qing Lu, Hai-Miao Hu, Jinzu Yu, Yibo Zhou, Hanzi Wang, and Bo Li. Orientation-aware pedestrian attribute recognition based on graph convolution network. *IEEE Transactions on Multimedia*, 26:28–40, 2023.

[26] Alec Radford, Jong Wook Kim, Chris Hallacy, Aditya Ramesh, Gabriel Goh, Sandhini Agarwal, Girish Sastry, Amanda Askell, Pamela Mishkin, Jack Clark, Gretchen Krueger, and Ilya Sutskever. Learning transferable visual models from natural language supervision. In *Proceedings of the 38th International Conference on Machine Learning*, pages 8748–8763. PMLR, 2021.

[27] Nikolaos Sarafianos, Xiang Xu, and Ioannis A Kakadiaris. Deep imbalanced attribute classification using visual attention aggregation. In *Proceedings of the European conference on computer vision (ECCV)*, pages 680–697, 2018.

[28] Jifeng Shen, Teng Guo, Xin Zuo, Heng Fan, and Wankou Yang. Sspnet: Scale and spatial priors guided generalizable and interpretable pedestrian attribute recognition. *Pattern Recognition*, 148:110194, 2024.

[29] Amit Singhal et al. Introducing the knowledge graph: things, not strings. *Official google blog*, 5(16):3, 2012.

[30] Zengming Tang and Jun Huang. Drformer: Learning dual relations using transformer for pedestrian attribute recognition. *Neurocomputing*, 497:159–169, 2022.

[31] Xiao Wang, Shaofei Zheng, Rui Yang, Aihua Zheng, Zhe Chen, Jin Tang, and Bin Luo. Pedestrian attribute recognition: A survey. *Pattern Recognition*, 121:108220, 2022.

[32] Xiao Wang, Jiandong Jin, Chenglong Li, Jin Tang, Cheng Zhang, and Wei Wang. Pedestrian attribute recognition via clip based prompt vision-language fusion. *IEEE Transactions on Circuits and Systems for Video Technology*, 2024.

[33] Xiao Wang, Weizhe Kong, Jiandong Jin, Shiao Wang, Rui-chong Gao, Qingchuan Ma, Chenglong Li, and Jin Tang. An empirical study of mamba-based pedestrian attribute recognition. *arXiv preprint arXiv:2407.10374*, 2024.

[34] Xiao Wang, Shiao Wang, Yuhe Ding, Yuehang Li, Wentao Wu, Yao Rong, Weizhe Kong, Ju Huang, Shihao Li, Haoxiang Yang, et al. State space model for new-generation network alternative to transformers: A survey. *arXiv preprint arXiv:2404.09516*, 2024.

[35] Junyi Wu, Yan Huang, Zhipeng Gao, Yating Hong, Jianqiang Zhao, and Xinsheng Du. Inter-attribute awareness for pedestrian attribute recognition. *Pattern Recognition*, 131:108865, 2022.

[36] Junyi Wu, Yan Huang, Min Gao, Zhipeng Gao, Jianqiang Zhao, Jieming Shi, and Anguo Zhang. Exponential information bottleneck theory against intra-attribute variations for pedestrian attribute recognition. *IEEE Transactions on Information Forensics and Security*, 18:5623–5635, 2023.

[37] Junyi Wu, Yan Huang, Min Gao, Yuzhen Niu, Mingjing Yang, Zhipeng Gao, and Jianqiang Zhao. Selective and orthogonal feature activation for pedestrian attribute recognition. In *Proceedings of the AAAI Conference on Artificial Intelligence*, pages 6039–6047, 2024.

[38] Junyi Wu, Yan Huang, Min Gao, Yuzhen Niu, Yuzhong Chen, and Qiang Wu. Enhanced visual-semantic interaction with tailored prompts for pedestrian attribute recognition. In *Proceedings of the Computer Vision and Pattern Recognition Conference*, pages 9570–9579, 2025.

[39] Junyi Wu, Yan Huang, Min Gao, Yuzhen Niu, Yuzhong Chen, and Qiang Wu. High-order diversity feature learning for pedestrian attribute recognition. *Neural Networks*, 188:107463, 2025.

[40] Shu Wu, Yuyuan Tang, Yanqiao Zhu, Liang Wang, Xing Xie, and Tieniu Tan. Session-based recommendation with graph neural networks. In *Proceedings of the AAAI conference on artificial intelligence*, pages 346–353, 2019.

[41] Yang Yang, Zichang Tan, Prayag Tiwari, Hari Mohan Pandey, Jun Wan, Zhen Lei, Guodong Guo, and Stan Z Li. Cascaded split-and-aggregate learning with feature recombination for pedestrian attribute recognition. *International Journal of Computer Vision*, 129(10):2731–2744, 2021.

[42] Junkun Yuan, Xinyu Zhang, Hao Zhou, Jian Wang, Zhong-wei Qiu, Zhiyin Shao, Shaofeng Zhang, Sifan Long, Kun Kuang, Kun Yao, et al. Hap: Structure-aware masked image modeling for human-centric perception. *Advances in Neural Information Processing Systems*, 36:50597–50616, 2023.

[43] Jialiang Zhang, Lixiang Lin, Jianke Zhu, Yang Li, Yun-chen Chen, Yao Hu, and Steven CH Hoi. Attribute-aware pedestrian detection in a crowd. *IEEE Transactions on Multimedia*, 23:3085–3097, 2020.

[44] Aihua Zheng, Huimin Wang, Jiaxiang Wang, Huabo Huang, Ran He, and Amir Hussain. Diverse features discovery transformer for pedestrian attribute recognition. *Engineering Applications of Artificial Intelligence*, 119:105708, 2023.

[45] Yibo Zhou, Hai-Miao Hu, Jinzu Yu, Zhenbo Xu, Weiqing Lu, and Yuran Cao. A solution to co-occurrence bias: Attributes disentanglement via mutual information minimization for pedestrian attribute recognition. *arXiv preprint arXiv:2307.15252*, 2023.

[46] Yibo Zhou, Hai-Miao Hu, Yirong Xiang, Xiaokang Zhang, and Haotian Wu. Pedestrian attribute recognition as label-balanced multi-label learning. *arXiv preprint arXiv:2405.04858*, 2024.

[47] Jialong Zuo, Jiahao Hong, Feng Zhang, Changqian Yu, Hanyu Zhou, Changxin Gao, Nong Sang, and Jingdong Wang. Plip: Language-image pre-training for person representation learning. *Advances in Neural Information Processing Systems*, 37:45666–45702, 2024.